Modulation of L-cysteine adsorption on graphene: the role of the Al, Si, P, S dopant and the vacancy

Huijuan Luo[1,2], Lu Zhang[1,2], Kai Zhang[1,2,*]

[1] *School of energy and environment, Inner Mongolia University of Sncience & Technology, Inner Mongolia 014010, China*

[2] *Key laboratory of efficient and clean combustion, Inner Mongolia 014010, China*

Abstract: Promoting the application potential of graphenes in biomolecule adsorption and detection is of great significance in the field of nanobiotechnology. In this paper, the density functional theory calculation was used to study the adsorption and sensing of L-cysteine on graphene-based compounds, single-vacancy and double-vacancy graphenes (XSV and XDV) doped with 3p-bolck elements (Al, Si, P, and S). Along with the dopant changing from Al to S, XSV exhibits decreasing exothermical chemisorption to endothermical chemi-sorption, while XDV exhibits decreasing exothermical chemisorption to endothermical physisorption. L-cysteine adsorption on XDV is weaker than corresponding adsorption on XSV. Valence electron number, and atomic ionization potential, modulated by the 3p-block dopant, and X-C interaction, modulated by the vacancy type, contribute to adsorption mechanism of L-cysteine on XGs. The study could facilitate applications of Al, Si, P and S doped graphenes in biosensing technology, biomolecule immobilization, bioseparation and other fields.

Keywords: Graphene**;** Adsorption**;** Biomolecules**;** L-cysteine; Density functional theory calculations

* ~~Corresponding au~~thors: Kai Zhang.

E-mail addresses: btzk@imust.edu.cn .

1. Introduction

Nanotechnology is a science and technology that studies the motion laws and interactions of material composition systems with sizes ranging from 0.1 to 100 nm, as well as the technical issues in possible practical applications. Compared with traditional sensors, the performance of nano-sensors has been greatly reduced in size and accuracy. More importantly, the use of nano-technology to make sensors is on the atomic scale, which greatly enriches the theory of sensors and promotes the sensors. The production level has broadened the application field of the sensor.

Graphene and its derivatives are promising materials in recent years, owing to their unique combination of crystallographic and electronic structures and facile modifications of the flexible structure [1-6]. Fascinating application potentials of graphene and its derivatives in biosensing [7], drug delivery [8], biocatalysis [9], enzyme engineering [10] etc., have been exploited and uncovered. Especially in the field of biosensing, Al, Si, P and S doped graphenes might act as a good sensor platform for L-cysteine.

Among all the graphene-related materials, Al, Si, P and S doped graphenes have been studied by many research efforts [11-13], accompanied with interesting findings. It has been demonstrated that Al-S doped graphenes could exhibit promising optoelectronic device applications [14-17], effective molecular adsorption of H_2 [18, 19], H_2O [20], CH_2O [21], effective ion adsorption for As (III) removal [22] as well as enhanced molecular catalysis of CO [23], NO [24], O_2 [25-27], N_2O [28, 29], H_2 [30] etc. However, exploration of Al-S doped graphenes in biomolecular applications is relatively rare [31, 32]. On another hand, as revealed by previous studies [33-37], both the dopant and the vacancy could show significant modulation on geometrical and electronic features of the doped graphenes. Thus vacancy effects are also investigated in our research. To ensure that the results in the study are comparable with our previous findings [32, 38], L-cysteine (L-cys) is the probe amino acid.

In the present work, adsorption of L-cys on the single-vacancy and double-vacancy graphenes doped with the 3p-block elements (Al, Si, P and S) was investigated by using dispersion corrected density functional theory calculations. The modulation of the 3p-block dopant type and the vacancy type on adsorption interactions, adsorption mechanism and sensitivity of the graphenic supports towards L-cys is uncovered. Our results could provide atomic-scale insights to facilitate graphenes application in nanobiotechnological and biosensing fields.

2. Modelling and calculation details

2.1. Models building

Substituting a C atom by an X (X=Al, Si, P or S) dopant at the centre of the pristine graphene 6×6×1 supercell, corresponding X doped single-vacancy graphene (XSV) was constructed. Substituting two C atoms by an X (X=Al, Si, P or S) dopant at the centre of the pristine graphene supercell, corresponding X doped double-vacancy graphene (XDV) was constructed.

Relaxed structures of XSV and XDV (X=Al-S) were obtained through DMol^3 geometrical optimization.

Three kinds of upright adsorption configurations of L-cys/XGs (X=Al-S), through the unprotonated S-end, O-end or N-end functional group, were constructed. L-cys was placed directly on top of the dopant in XGs (X=Al-S) through the linking atom (S, O (O in OH) or N) at an initial distance of 3 Å. The upright adsorption configuration could facilitate polymerization through the free amino or carbonxyl group or incorporation of metal ions through the other two free functional groups [39-41]. The S-, O- and N-end L-cys/graphene adducts were marked as S-, O-, N-XSV and S-, O-, N-XDV for XSV and XDV, respectively. Stable adsorption configurations were achieved through full relaxation.

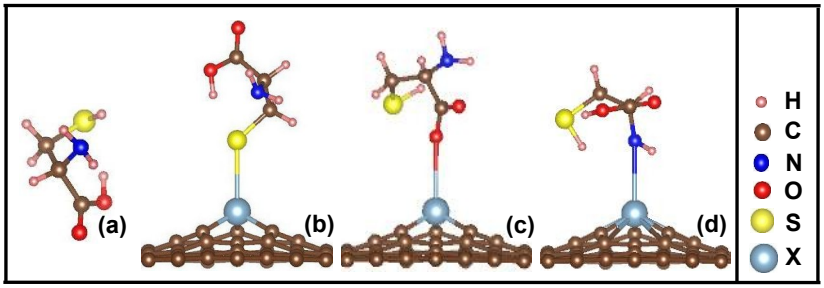

Figure 1 Schematic illustration of the L-cys molecule (a), and initial adsorption configurations of the S-end (b), O-end (c) and N-end (d) L-cys on XGs (X=Al-S).

2.2. Calculation parameters

Structural optimizations and electronic structure calculations were conducted by using the DMol^3 module in Materials Studio [42], as in our previous research [32, 38, 43]. The PBE of GGA functional was used for exchange-correlation effects. To include van der Waals interactions, standard parameter set of Grimme correction [44] were introduced to include van der Waals interactions. The dual-valued base set enhanced by the polarization function (DNP) is used as the base set. The DFT half-core pseudo-potential (DSPP) core processing was implemented. The convergence tolerances for geometrical optimization are 1.0×10^{-5} Hartree on energy, 1.0×10^{-3} Å^{-1} Hartree on gradient and 1.0×10^{-3}Å on displacement, respectively. The convergence criterion for self-consistent field (SCF) cycles is 1.0×10^{-6} e Å^{-3}.

2.3. Binding energy

To evaluate the stability of graphenic supports for L-cys docking, the binding energies (E_b) and the formation energies (E_f) of XSVs and XDVs were calculated [27] as follows.

$$E_b = E_{XSV} - E_X - E_{SV} \quad (1)$$

$$E_b = E_{XDV} - E_X - E_{DV} \quad (2)$$

where E_{XSV} and E_{XDV} represent the total energy of the optimized XSV and XDV, E_X the total energy

of an isolated X dopant, E_{SV} and E_{DV} the total energy of the reconstructed single-vacancy and double-vacancy graphene, respectively. The more negative value of E_b indicates more structural stability and larger binding strength [45].

$$E_f = E_{XSV/XDV} - E_G - \mu_X + n\mu_C \quad (3)$$

where $E_{XSV/XDV}$ and E_G are the total energies of the Al, Si, P and S doped graphene and the intrinsic graphene, respectively, while μ_X and μ_C are the chemical potentials of the substitutional and of the substituted host C atom, respectively. The chemical potentials are calculated with respect to the bulk crystal reference levels.

With respect to adsorption stability of L-cys on XG systems, the adsorption energy E_{ads} was calculated [46, 47] as

$$E_{ads} = E_{tot} + 1/2\, E_{H2} - E_{XG} - E_{L-cys} \quad (4)$$

where E_{tot} represents the total energy of the optimized L-cys/XG adduct, E_{XG} the total energy of XG, $E_{L\text{-}cys}$ the total energy of an isolated L-cys molecule, and E_{H2} the total energy of a hydrogen molecule, respectively. Unprotonated L-cys is not the most stable species in the gas phase. It is assumed that the hydrogen atoms dissociated from L-cys form molecules. Thus the total energy E_{H2} of the gas-phase H_2 molecule [46, 47] was considered. The more negative value of E_{ads} means a more favourable adsorption configuration.

3. Results and discussion

3.1. Basic properties of XGs (X=Al-S)

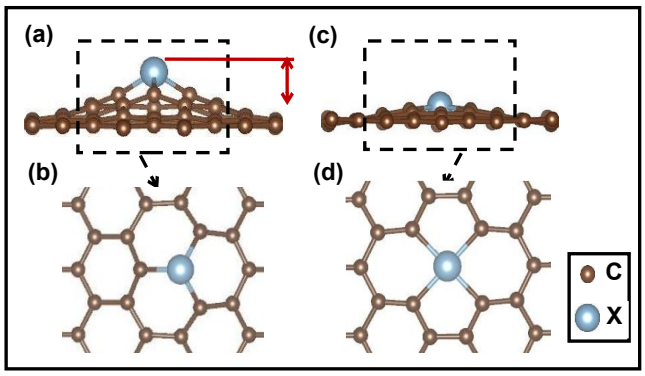

Figure 2 Schematic illustration of optimized XSVs (X=Al-S): side view (a), top view (b) and optimized XDVs: side view (c), top view (d). *h* denotes elevation of the X dopant, relative to average height of graphenic carbon atoms.

Typical relaxed configurations of the 3p-block elements doped XSVs (X=Al-S) are shown in Figure 2 (a, b). The E_b values (Figure 3(a)) distribute in the range of -10 ~ -5 eV, indicating strong doping ability. Along with the dopant changing from Al to S, a non-monotonic change behaviour appears. The largest binding strength among them is found for SiSV, attributed to saturation of four valence electrons (Si: $3s^2 3p^2$). Three valence electrons go into the covalent Si-C σ bonds, and the fourth replaces the π electron of the missing carbon atom [34]. For all XSVs, the X dopant is displaced to a distance outwards (Figure 2(a)) from the graphenic surface due to a larger atomic radius relative to carbon. The elevation *h* of the dopants is exhibited in Figure 3(b). Surrounding carbon atoms are also distracted outwards, thus facilitating formation of three equivalent X-carbon (X-C) bonds [48]. The average X-C bond lengths (Figure 3(c)) are all below the sum of covalent radii [49] of the corresponding X

dopant and C, in consistence with strong doping strengths.

For XDVs, the E_b values distribute in the range of -9 ~ -5 eV, indicating good structural stability. From Al to S, a non-monotonic change behaviour occurs. SiDV exhibits the largest doping ability, with four valences saturated [34]. All XDVs (X=Al-S) exhibit a "cross" configuration (Figure 2(d)), with the dopant equivalently bonded to neighbouring four carbon atoms. The Al dopant is obviously elevated, while Si, P and S dopants almost remain in the graphenic plane (Figure 3 (b)). For all 3p-block dopants, the X-C bonding length is larger than the sum of covalent radii of X and C (Figure 3(c)). Comparison of the E_b values and X-C bonding lengths of XSVs and XDVs shows that the introduction of bigger vacancies leads to more separation between the 3p-block dopants (X=Al-S) and neighbouring carbon atoms, and thus less X-C interactions are accompanied [33].

Compared to the cohesive energies of the Al, Si, P or S bulk crystal [50], the binding energies are more negative. This shows that the Al, Si, P or S atom could be stably trapped into graphene without clustering. When vacancy formation is considered, the calculated formation energies are in the range of 2.49 ~ 4.44 eV. The large formation energies indicate intrinsic graphene is much stable, and the formation of Al, Si, P or S doped graphenes is endothermic. For single vacancy formation, the formation energy is 7.7 eV [51], showing that Al, Si, P or S-doping could occur easily than C-vacancy formation in the stable lattice of graphene. Regarding fabrication of Al, Si, P or S doped graphenes, the two-step route could be considered [52]. Firstly, under He^+ ion beam bombardment, high density monovacancies are created. Secondly, a short-time sputtering is followed.

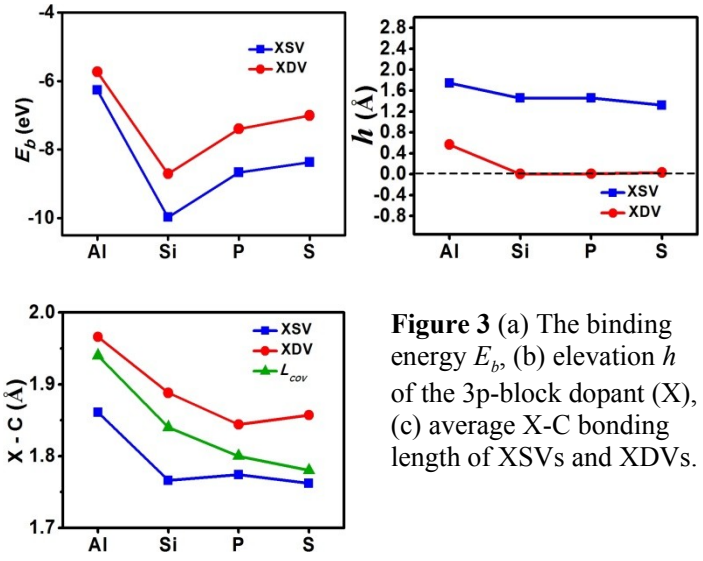

Figure 3 (a) The binding energy E_b, (b) elevation h of the 3p-block dopant (X), (c) average X-C bonding length of XSVs and XDVs.

Table 1

Cohesive energies (E_c), binding energies (ΔE_b) and formation energies (E_f) of Al, Si, P and S doped graphenes.

XSV	E_c(eV)	ΔE_b(eV)	E_f(eV)
AlSV	-3.39	-6.26	4.17
SiSV	-4.63	-9.97	2.65
PSV	-3.43	-8.67	2.49
SSV	-2.65	-8.36	2.66
XDV	E_c(eV)	ΔE_b(eV)	E_f(eV)
AlDV	-3.39	-5.73	4.44
SiDV	-4.63	-8.71	3.66
PDV	-3.43	-7.39	3.50
SDV	-2.65	-7.00	3.75

3.2. Adsorption stability of the L-cys/XG adducts

3.2.1. Adsorption stability of the L-cys/XSV adducts

For L-cys/XSVs, the E_{ads} values (Figure 4) exhibit a transition from negative to positive values with the X dopant changing from Al to S. AlSV, SiSV and PSV show exothermic adsorption towards L-cys, regardless of the end type. Large electron transfer in charge difference density distribution (Figure 5(a-c)) further indicates the existence of stable exothermic chemisorptions. SSV shows endothermic adsorption towards the S-end L-cys (0.34 eV), O-end L-cys (0.46 eV) and N-end L-cys (1.24 eV). Although E_{ads} values are larger than zero, large electron transfer in charge difference density distribution (Figure 5(d) and Figure S1) suggests SSV exhibits endothermic chemisorptions towards L-cys.

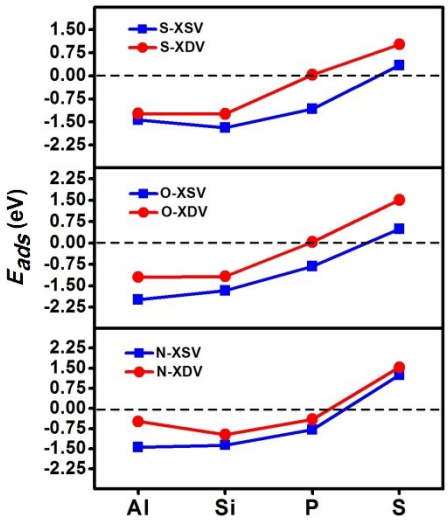

Figure 4 E_{ads} of L-cys/XSVs and L-cys/XDVs with different end-types of L-cys adsorbed.

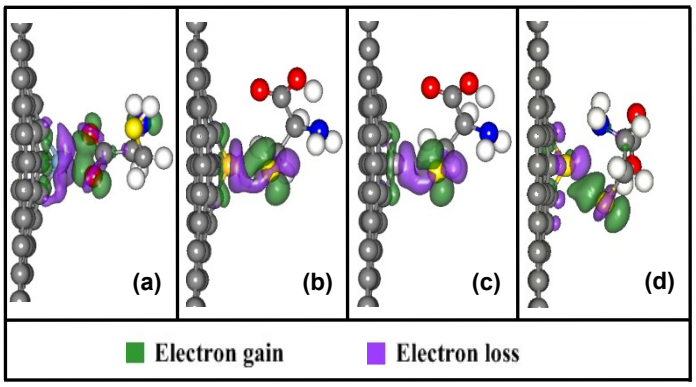

Figure 5 Charge density difference graphs of the most stable adsorptions on XSVs: (a) O-AlSV, (b) S-SiSV, (c) S-PSV, (d) S-SSV.

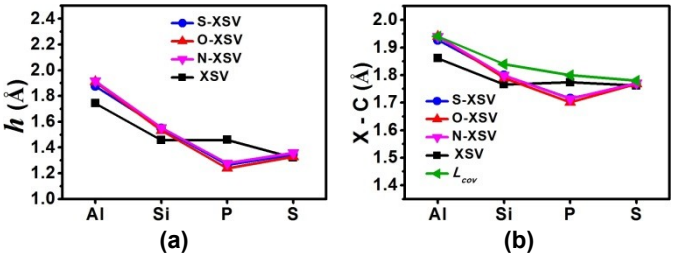

Figure 6 (a) The elevation h of the X dopant and (b) the average X-C bonding length in XSVs. L_{COV} indicates the sum of the covalent radii of X and C.

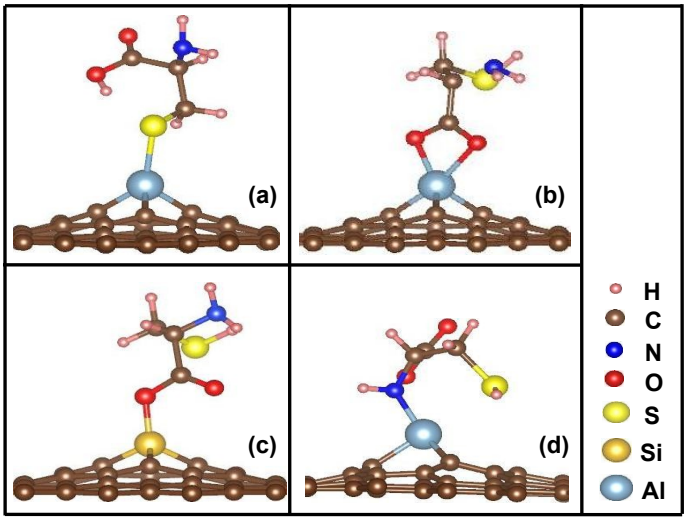

Figure 7 Typical adsorption geometries of L-cys on XGs to illustrate the one-site S-end linking (a), two-site O-end linking (b), one-site O-end linking (c) and one-site N-end linking (d).

The XSV (X=Al-S) substrate can withstand strain relaxation, thereby contributing to adsorption stability (Figure 6). For different 3p-block dopants, the position of the dopant (Figure 6(a)) and adjacent carbon atoms changed significantly, and the average X-C bond length also changed (Figure 6(b)). Concerning L-cys/AlSV and L-cys/SiSV, Al and Si dopants are further elevated [43], and the corresponding average X-C length is elongated to approach the sum of the covalent radii. In L-cys/PSV adducts, the P dopant is pushed downwards towards the graphenic plane and the P-C bond is shortened to much less than the sum of the covalent radii. For L-cys/SSV, the position of the S dopant and the X-C bonding length are almost unchanged, in consistence with weak adsorption. As for L-cys, most of the bond lengths and bond angles remain almost unchanged after adsorption. The angles related to adsorbed functional groups are greatly changed.

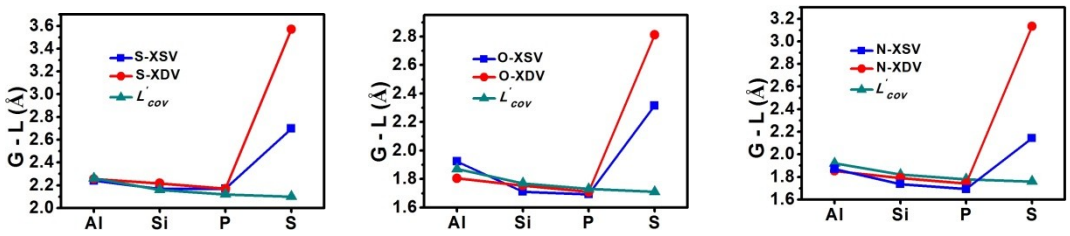

Figure 8 The G-L bonding length through the (a) S-, (b) O- and (c) N-end docking. L'_{COV} indicates the sum of the covalent radii of X and the linking atom in L-cys.

One-site S-end chemisorption appears for all S-XSV adducts, with formation of the covalent X-S bond (Figure 7(a)), the -COOH and -NH_2 groups free extending outwards. Regarding O-end adduction, AlSV shows bi-O (binding through O in OH and O in O=) adsorption (Figure 7(b)), with two equal Al-O bonds (2.00 Å). A large steric hindrance, arising from the two Al-O bonds, exists to keep the upright adsorption configuration robust. Differently, Si, P and S doped single vacancy graphenes favour a mono-O adsorption mode (Figure7(c)), with chemical bonding through O in OH. Regarding the N-end addition, all XSVs have a single point of adsorption through the formation of X-N covalent bonds, and -COOH and -SH extend freely outward (Figure 7(d)). For any three adducts, the bonding distance between L-cys and graphene substrate (G-L) decreases monotonically from AlSV to PSV, and increases dramatically for SSV (Figure 8(a-c)).

3.2.2. Adsorption stability of the L-cys/XDV adducts

With respect to L-cys docking on XDVs, the E_{ads} values (Figure 4) also show an interesting transition from negative to positive values along with the 3p-block dopant changing from Al to S. For L-cys docking on XDV (X=Al, Si), all related E_{ads} values are less than zero, showing exothermic adsorption towards the three kinds of L-cys radicals. Large electron transfer in charge difference density distribution (Figure 9(a-b)) indicates the existence of stable exothermic chemisorptions. PDV shows exothermic chemisorption (Figure 9(c))

towards the N-end L-cys (-0.41 eV) and endothermic chemi-sorptions (Figure S2) towards the O-end (0.04 eV) and S-end (0.04 eV) L-cys. SDV shows endothermic physisorption towards all the three kinds of L-cys radicals, accompanied with no overlap in charge difference density distribution (Figure 9(d)). X (X=Al-P) doped double-vacancy graphenes show good reactivity, while SDV shows inert reactivity towards L-cys. The findings would provide a meaningful theoretical reference in practical applications about selecting appropriate dopants for physisorption or chemisorption towards adsorbates.

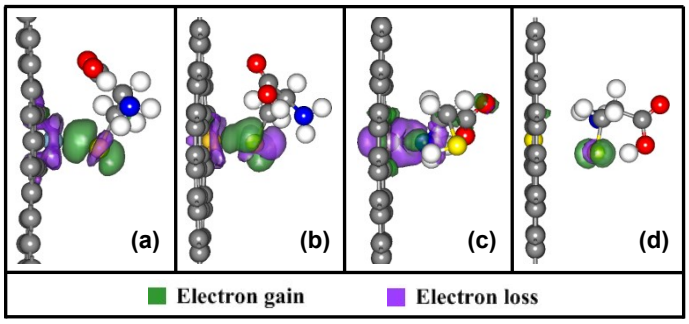

Figure 9 Charge density difference graphs of the most stable adsorption on XDVs: (a) S-AlDV, (b) S-SiDV, (c) N-PDV, (d) S-SDV.

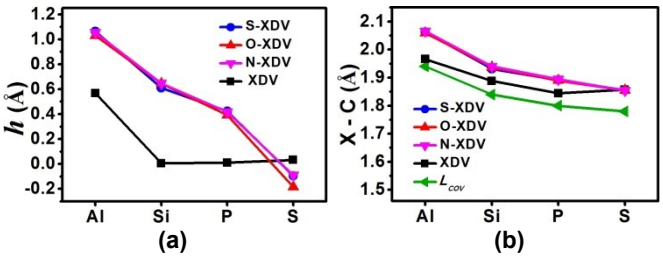

Figure 10 (a) The elevation *h* of the 3p-block dopant (X) and (b) the average X-C bonding length in XDVs. L_{COV} indicates the sum of the covalent radii of X and C.

The graphenic substrates of XDVs also undergo geometrical distortions to facilitate L-cys adsorption. From Al to P, the 3p-block dopants are obviously elevated (Figure 10(a)), with neighbouring carbon atoms largely protruded out by L-cys. This leads to longer X-C bonding length (Figure 10(b)) and much weaker X-C bonding strength. For SDV, S is mildly excluded by L-cys, with the movement of *h* in an opposite direction. The S-C bonding length is unchanged. For all adsystems on XDVs (X=Al-S), no obvious structural changes appear in L-cys.

For the S-end, O-end and N-end adductions, all L-cys/XDV adsystems show one-site docking, with a single X-S, X-O (O in OH) and X-N binding (Figure 7(a)). The bonding distance between L-cys and the graphenic substrate (G-L) monotonously decreases from AlDV to PDV, then increases dramatically for SDV (Figure 8(a-c)), regardless of the docking end type.

3.2.3. Site-specific adsorption phenomena

Herein, site-specific chemisorption (Table 2) is revealed by analysis of the most stable adsorption configurations. In the case of single-vacancy graphenes, the S-terminal L-cys docking on Si-S doped graphenes is stronger than the -COOH or -NH_2 but the O-end L-cys exhibits the most on Al doped Good adsorption stability. Single vacancy graphene. In the case of double-vacancy graphene, the S-terminal L-cys docking on Al, Si and S doped graphenes is stronger than -COOH or -NH_2, while the N-end L-cys performs best on P stability. That is to say, for SiG and SG, regardless of the type of vacancy, the S-end immobilization showed the strongest affinity. For AlG and PG, the adsorption affinity

is easily affected by the vacancy. Therefore, site-specific chemisorptions could be achieved through modification of the kind of the 3p-block dopant and the vacancy in the graphene support.

Table 2

The most stable adsorptions on XGs (X=Al-S).

	Al	Si	P	S
XSV	O	S	S	S
XDV	S	S	N	S

3.2.4. Adsorption mechanism analysis

The adsorption mechanism could be understood from the following aspects: (i) the 3p-block dopants, which possess different numbers of outer-shell 3p electrons and different ionization potentials; (ii) the vacancy types, which contribute different X-C interactions between the 3p-block dopant and neighbouring carbon atoms.

It was proposed in our previous research [38] that V ($3d^3 4s^2$), owing five valence electrons, doped graphenes exhibits the most stable adsorptions among all the 3d transition metal doped graphenes, regardless of the vacancy type. This is attributed to saturation of valence electrons (Figure 11(a, b)). Differently, in this study, P ($3s^2 3p^3$), owing five valence electrons, doped graphenes exhibit weaker adsorption stability relative to Al and Si doped graphenes, even with the occurrence of endothermic adsorptions. This is due to the influence of atomic ionization potential, which represents atoms losing electron ability. As shown in Figure 11(c, d), the dopants lose electron to facilitate L-cys adsorption. From Al to S, atomic ionization potential (Table 3) exhibits a monotonically increasing tendency, thus the ability of losing electron monotonically decreases. For PSV and PDV, the influence of high ionization potential exceeds the influence of valence electron saturation, thus exhibiting weaker adsorption strength towards L-cys, compared to AlG and SiG. Owing to valence electron abundance [38] and high ionization potential, SSV exhibits endothermic chemisorptions and SDV exhibits physisorption towards L-cys.

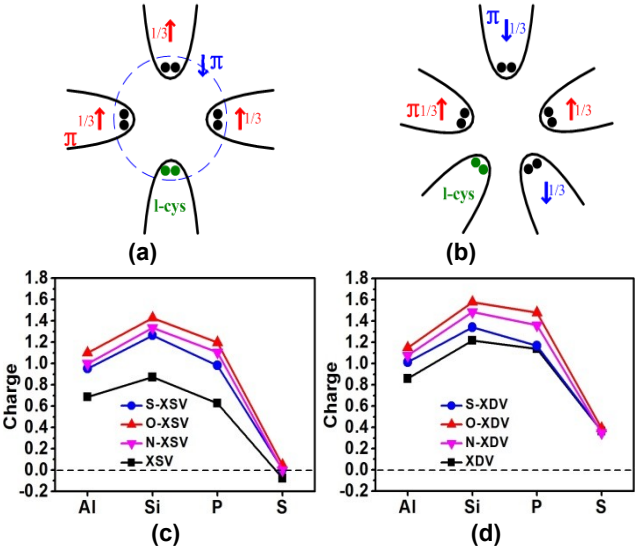

Figure 11 Schematic of the ideal electronic structure of L-cys/PSV (a) and L-cys/PDV (b) complexes. Charge of the dopant X in (c) XSVs, L-cys/XSVs and (d) XDVs, L-cys/XDVs (X=Al, Si, P, S). In (a) and (b), the number "1/3" symbolically represents ligand contribution to the approximate π bond, because one π electron is shared among three π bonds.

The role of vacancy is deduced from weaker adsorption on Al-S doped double-vacancy graphenes than single-vacancy graphenes, regardless of the docking end group. In doped double-vacancy graphenes, the longer X-C bonding lengths (Figure

S3) lead to weaker X-C interactions, thus less contribution of neighbouring carbon atoms towards L-cys adsorption.

Compared to our previous finding [38], it is noted that a new atomic indicator, ionization potential, play an important role in influencing L-cys adsorption. The finding here will provide a good reference standard for choosing appropriate graphenic supports for amino acids adsorption.

Table 3

Ionization potentials [44] of the 3p-block elements.

	Ionization potential/ kJ mol^{-1}
Al	577.6
Si	786.4
P	1011.7
S	999.6

3.3. Sensor sensitivity analysis

In order to evaluate the sensitivity of doped graphenes, we calculated the sensor sensitivity of Al, Si, P , S doped single vacancy and double vacancy graphenes towards -SH, -NH_2 and -COOH L-cys, respectively (Figure 12). We compared the sensor sensitivities of single vacant graphene doped with Al, Si, P, and S (Figure 12 (a)), and found that the sensitivity of the sensor adsorbed by -SH, -NH_2, and -COOH in the single element doped by Si is inene close to each other, the sensitivity is about 300%, and the same pattern is found in the P element. The sensitivity of the sensor is about 70%. The Al-doped single-vacancy graphene has the highest sensitivity at the -NH_2 terminal, which is 14.32%. The adsorption sensitivity of -COOH in S-doped single vacancy graphene is significantly higher than that of -SH and -NH_2. The highest sensitivity of doped single-vacancy graphene is 305.86%, and the lowest sensitivity is 1.05%. By comparing the sensitivity of the L-cys sensor adsorbed by four elements in XDV (Figure 12 (b)), it was found that the sensitivity of O-AlDV and O-SDV sensors is higher than that of S-AlDV, N-AlDV and S-AlDV, N-AlDV However, in the sensor sensitivity of Si, P-doped graphene, O-SiDV and O-PDV are lower than S-SiDV, N-SiDV and S-PDV, N-PDV. The highest sensitivity of doped double-vacancy graphene is 263.88%, while the lowest is 15.50%.

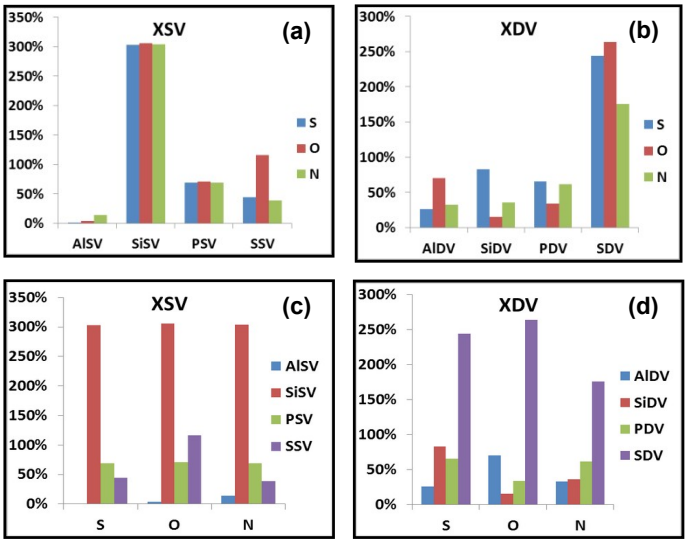

Figure 12 The sensitivity of XSV and XDV to L-cys sensor: (a) Sensitivity of Al-S doped single vacancy graphene, (b) Sensor sensitivity of Al-S doped double vacancy graphene, (c) Sensor sensitivity of -SH, -NH_2 and -COOH L-cys adsorption on single vacancy graphene, (d) Sensor sensitivity of -SH, -NH_2 and -COOH L-cys adsorption on double vacancy graphene.

The sensitivity of AlSV, SiSV, PSV, and SSV adsorbed at the -SH, -NH_2, and -COOH ends of L-

cys was compared (Figure 12 (c)). It was found that the sensitivity of SiSV was significantly higher than that of AlSV, PSV, and SSV, and the sensitivity of adsorption on -COOH terminal was as high as 305.86%. AlSV has the lowest sensitivity, especially adsorbed on the -SH end. By comparing the adsorption sensitivities of L-cys -SH terminal, -NH_2 terminal and -COOH terminal on double-vacancy graphene (Figure 12 (d)), it was found that S element adsorbed on the -SH terminal, -NH_2 terminal and -COOH sensor The sensitivity is significantly higher than the sensitivity of the other three elements at the -SH, -NH_2 and -COOH, and the highest sensitivity reaches 263.88%.

4. Conclusions

The present study investigates modulation of the 3p-block dopant type and the vacancy type on the interactions between L-cys and Al-S doped graphenes using the DFT-D approach. This work could provide atomic-scale insights into applications of Al-S doped graphenes in biosensing, biomolecules immobilization, magnetic bio-separation and other bionanotechnological fields. The main conclusions are summarized as follows:

(i) The 3p-block dopant (Al-S) exhibit different reactivity modulation, leading to exothermical chemisorptions, endo-thermical chemisorptions and endo-thermical physisorptions of the graphenic support towards L-cys. Meanwhile, site-specific adsorption towards L-cys is obtained. Preference to docking through the S-end L-cys appears for most doped graphenes. AlSV and PDV show the strongest affinity towards the O-end and N-end L-cys, respectively.

(ii) Along with the 3p-block dopant chaning from Al to S, nearly decreasing variation tendency in adsorption energies occurs for L-cys adduction on XSVs and XDVs. L-cys adsorption on XDVs is weaker than corresponding adsorption on XSVs.

(iii) Adsorption mechanism analysis reveals that atomic indicators, including the valence electron number and ionization potential, and the vacancy type together play important roles in L-cys adsorption stability.

(iv) The sensor element Si doped with single-vacancy graphene is superior to the other three elements, while the sensor element S doped with double-vacancy graphene is superior to the other three elements.

On the basis of the aforementioned conclusions, specific applications of the 3p-block dopant (Al-S) doped graphenes could be expected. AlG and SiG could act as a good immobilization platform toward L-cysteine. P and S doped graphenes might act as a good sensor platform for L-cysteine. Through tuning the dopant and the vacancy type in doped graphene, site-specific immobilization could be realized. PDV could work in specific N-end adsorption applications.

Declaration of Competing Interest

The authors declare that they have no known competing financial interests or personal

relationships that could have appeared to influence the work reported in this paper.

Funding Information

This work was supported by the Inner Mongolia Natural Science Foundation-Major Project [Grant No. 2019ZD13]; the IMAR (Inner Mongolia Autonomous Region) Natural Science Foundation [Grant No. 2019MS02005, 2018LH05013, 2018MS02013, 2018LH05016]; the Inner Mongolia Major Basic Research Open Project [Grant No. 0406091701] and the Innovation Fund Project of Inner Mongolia University of Science and Technology [2017QDL-B16].

References

[1] D. Cortés-Arriagada, D. E. Ortega (2018) Effects on the aromatic character of DNA/RNA nucleobases due to its adsorption onto graphene, Int. J. Quantum Chem. 118:e25699. https://doi.org/10.1002/qua.25699

[2] Q. Li, H. Wang, H. Xia, S. Wei, J. Yang (2014) Density functional study of hydrogen adsorption and diffusion on Ni−loaded graphene and graphene oxide, Int. J. Quantum Chem. 114:879. https://doi.org/10.1002/qua.24680

[3] D. Cortés-Arriagada (2017) Adsorption of polycyclic aromatic hydrocarbons onto graphyne: Comparisons with graphene, Int. J. Quantum Chem. 117:e25346. https://doi.org/10.1002/qua.25346

[4] N. Javadi, M. Najafi, S. Yourdkhani (2017) On the role of substituent in noncovalent functionalization of graphene and organophosphor recognition: IQA and SAPT perspective, Int. J. Quantum Chem. 117:e25379. https://doi.org/10.1002/qua.25379

[5] M. D. Esrafili, R. Nurazar, E. Vessally (2015) Application of Si−doped graphene as a metal-free catalyst for decomposition of formic acid: A theoretical study, Int. J. Quantum Chem. 115:1153. https://doi.org/10.1002/qua.24942

[6] G. Fazio, L. Ferrighi, D. Perilli, C. D. Valentin (2016) Computational electrochemistry of doped graphene as electrocatalytic material in fuel cells, Int. J. Quantum Chem. 116: 1623. https://doi.org/10.1002/qua.25203

[7] M.S. Artiles, C.S. Rout, T.S. Fisher (2011) Graphene-based hybrid materials and devices for biosensing, Adv. Drug Deliver. Rev. 63:1352-1360.https://doi.org/10.1016/j.addr.2011.07.005

[8] L. Tang, Y. Wang, J. Li (2015) The graphene/nucleic acid nanobiointerface, Chem. Soc. Rev. 44:6954-6980. https://doi.org/10.1039/C4CS00519H

[9] A. Karimi, A. Othman, A. Uzunoglu, L. Stanciu, S. Andreescu (2015) Graphene based enzymatic bioelectrodes and biofuel cells, Nanoscale 7:6909-6923.https://doi.org/10.1039/C4NR07586B

[10] Y. Tu, M. Lv, P. Xiu, T. Huynh, M. Zhang, M. Castelli, Z. Liu, Q. Huang, C. Fan, H. Fang, R. Zhou (2013) Destructive extraction of phospholipids from Escherichia coli membranes by graphene nanosheets, Nat. Nanotechnol. 8:594-601. https://doi.org/10.1038/nnano.2013.125

[11] P.A. Denis (2011) When noncovalent interactions are stronger than covalent bonds: Bilayer graphene doped with second row atoms, aluminum, silicon, phosphorus and sulfur, Chem. Phys. Lett. 508:95-101. https://doi.org/10.1016/j.cplett.2011.04.018

[12] J. Dai, J. Yuan, P. Giannozzi (2009) Gas adsorption on graphene doped with B, N, Al, and S: A theoretical study, Appl. Phys. Lett. 95:232105. https://doi.org/10.1063/1.3272008

[13] H. Wang, H. Wang, Y. Chen, Y. Liu, J. Zhao, Q. Cai, X. Wang (2013) Phosphorus-doped graphene and (8, 0) carbon nanotube: Structural, electronic, magnetic properties, and chemical reactivity, Appl. Surf. Sci. 273:302-309. https://doi.org/10.1016/j.apsusc.2013.02.035

[14] M. Houmad, H. Zaari, A. Benyoussef, A. El Kenz, H. Ez-Zahraouy (2015) Optical conductivity enhancement and band gap opening with silicon doped graphene, Carbon 94:1021-1027. https://doi.org/10.1016/j.carbon.2015.07.033

[15] M.E. Mikko, Z.Y. Fan, A. Uppstu, A.V. Krasheninnikov, A. Harju (2015) Silicon and silicon-nitrogen impurities in graphene: Structure, energetics, and effects on electronic transport, Phys. Rev. B 92:235412. https://doi.org/10.1103/PhysRevB.92.235412

[16] S.J. Zhang, S.S. Lin, X.Q. Li, X.Y. Liu, H.A. Wu, W.L. Xu, P. Wang, Z.Q. Wu, H.K. Zhong, Z.J. Xu (2016) Opening the band gap of graphene through silicon doping for the improved performance of graphene/GaAs heterojunction solar cells†, Nanoscale 8:226-232. https://doi.org/10.1039/C5NR06345K

[17] S. Some, J. Kim, K. Lee, A. Kulkarni, Y. Yoon, S. Lee, T. Kim, H. Lee (2012) Highly Air-Stable Phosphorus-Doped n-Type Graphene Field-Effect Transistors, Adv. Mater. 24:5481-5486. https://doi.org/10.1002/adma.201202255

[18] J. Carrete, R.C. Longo, L.J. Gallego, A. Vega, L.C. Balbás (2012) Al enhances the H_2 storage capacity of graphene at nanoribbon borders but not at central sites: A study using nonlocal van der Waals density functionals, Phys. Rev. B 85:125435. https://doi.org/10.1103/PhysRevB.85.125435

[19] H. Zhang, X. Luo, X. Lin, X. Lu, Y. Leng (2013) Density functional theory calculations of hydrogen adsorption on Ti-, Zn-, Zr-, Al-, and N-doped and intrinsic graphene sheets, Int. J. Hydrogen Energy 38:14269-14275. https://doi.org/10.1016/j.ijhydene.2013.07.098

[20] Q.G. Jiang, Z.M. Ao, Q. Jiang (2013) First principles study on the hydrophilic and conductive graphene doped with Al atoms, Phys. Chem. Chem. Phys. 15:10859-10865. https://doi.org/10.1039/C3CP00128H

[21] M. Chi, Y. Zhao (2009) Adsorption of formaldehyde molecule on the intrinsic and Al-doped graphene: A first principle study, Comp. Mater. Sci. 46:1085-1090. https://doi.org/10.1016/j.commatsci.2009.05.017

[22] D. Cortes-Arriagada, A. Toro-Labbe (2015) Improving As(iii) adsorption on graphene based surfaces: impact of chemical doping†, Phys. Chem. Chem. Phys. 17:12056-12064. https://doi.org/10.1039/C5CP01313E

[23] Y. Tang, Z. Liu, X. Dai, Z. Yang, W. Chen, D. Ma, Z. Lu (2014) Theoretical study on the Si-doped graphene as an efficient metal-free catalyst for CO oxidation, Appl. Surf. Sci. 308:402-407. https://doi.org/10.1016/j.apsusc.2014.04.189

[24] Y. Chen, Y.J. Liu, H.X. Wang, J.X. Zhao, Q.H. Cai, X.Z. Wang, Y.H. Ding (2013) Silicon-Doped Graphene: An Effective and Metal-Free Catalyst for NO Reduction to N_2O, ACS Appl. Mater. Interfaces 5:5994-6000. https://doi.org/10.1021/am400563g

[25] Z. Yang, Z. Yao, G. Li, G. Fang, H. Nie, Z. Liu, X. Zhou, X. Chen, S. Huang (2012) Sulfur-Doped Graphene as an Efficient Metal-free Cathode Catalyst for Oxygen Reduction, ACS Nano 6:205-211. https://doi.org/10.1021/nn203393d

[26] J.C. Wang, R.G. Ma, Z.Z. Zhou, G.H. Liu, Q. Liu (2015) Magnesiothermic synthesis of sulfur-doped graphene as an efficient metal-free electrocatalyst for oxygen reduction, Sci. Rep. 5:9304. https://doi.org/10.1038/srep09304

[27] M.A. Hoque, F.M. Hassan, M.H. Seo, J.Y. Choi, M. Pritzker, S. Knights, S.Y. Ye, Z.W. Chen (2016) Optimization of sulfur-doped graphene as an emerging platinum nanowires support for oxygen reduction reaction, Nano Energy 19:27-38. https://doi.org/10.1016/j.nanoen.2015.11.004

[28] Y.A. Lv, G.L. Zhuang, J.G. Wang, Y.B. Jia, Q. Xie (2011) Enhanced role of Al or Ga-doped graphene on the adsorption and dissociation of N_2O under electric field, Phys. Chem. Chem. Phys. 13:12472-12477. https://doi.org/10.1039/C1CP20694J

[29] R. Gholizadeh, Y. Yu (2015) N_2O + CO reaction over Si- and Se-doped graphenes: An ab initio DFT study, Appl. Surf. Sci. 357:1187-1195. https://doi.org/10.1016/j.apsusc.2015.09.163

[30] R.K. Shervedani, A. Amini (2015) Sulfur-doped graphene as a catalyst support: Influences of carbon black and ruthenium nanoparticles on the hydrogen evolution reaction performance, Carbon 93:762-773. https://doi.org/10.1016/j.carbon.2015.05.088

[31] S.K. Mudedla, K. Balamurugan, M. Kamaraj, V. Subramanian (2016) Interaction of nucleobases with silicon doped and defective silicon doped graphene and optical properties†, Phys. Chem. Chem. Phys. 18:295-309. https://doi.org/10.1039/C5CP06059A

[32] H. Luo, H. Li, Q. Fu, Y. Chu, X. Cao, C. Sun, X. Yuan, L. Liu (2013) Density functional theory study on the interactions of l-cysteine with graphene: adsorption stability and magnetism, Nanotechnology 24:495702. https://doi.org/10.1088/0957-4484/24/49/495702

[33] A.V. Krasheninnikov, P.O. Lehtinen, A.S. Foster, P. Pyykkö, R.M. Nieminen (2009) Embedding Transition-Metal Atoms in Graphene: Structure, Bonding, and Magnetism, Phys. Rev. Lett. 102:126807. https://doi.org/10.1103/PhysRevLett.102.126807

[34] A.W. Robertson, B. Montanari, K. He, J. Kim, C.S. Allen, Y.A. Wu, J. Olivier, J. Neethling, N. Harrison, A.I. Kirkland, J.H. Warner (2013) Dynamics of Single Fe Atoms in Graphene Vacancies, Nano Lett. 13:1468-1475. https://doi.org/10.1021/nl304495v

[35] H. Wang, Q. Wang, Y. Cheng, K. Li, Y. Yao, Q. Zhang, C. Dong, P. Wang, U. Schwingensschlogl, W. Yang, X.X. Zhang (2012) Doping Monolayer Graphene with Single Atom Substitutions, Nano Lett. 12:141-144. https://doi.org/10.1021/nl2031629

[36] L. Tsetseris, B. Wang, S.T. Pantelides (2014) Substitutional doping of graphene: The role of carbon divacancies, Phys. Rev. B 89:035411. https://doi.org/10.1103/PhysRevB.89.035411

[37] X. Hu, F. Meng (2016) Structure and gap opening of graphene with Fe doped bridged trivacancy, Comp. Mater. Sci. 117:65-70. https://doi.org/10.1016/j.commatsci.2015.12.025

[38] H. Luo, H. Li, Z. Xia, Y. Chu, J. Zheng, Z. Hou, Q. Fu (2016) Novel insights into l-cysteine adsorption on transition metal doped graphene: influences of the dopant and the vacancy†, RSC Adv. 6:29830-29839. https://doi.org/10.1039/C5RA25599F

[39] A. Liu, D. Chen, C. Lin, H. Chou, C. Chen (1999) Application of Cysteine Monolayers for Electrochemical Determination of Sub-ppb Copper(II), Anal. Chem. 71:1549-1552. https://doi.org/10.1021/ac980956g

[40] A. Kühnle, T.R. Linderoth, M. Schunack, F. Besenbacher (2006) l-Cysteine Adsorption Structures on Au(111) Investigated by Scanning Tunneling Microscopy under Ultrahigh Vacuum Conditions, Langmuir 22:2156-2160. https://doi.org/10.1021/la052564s

[41] Z. Zhang, H. Jia, F. Ma, P. Han, X. Liu, B. Xu (2011) First principle study of cysteine molecule on intrinsic and Au-doped graphene surface as a chemosensor device, J. Mol. Model. 17:649-655. https://doi.org/10.1007/s00894-010-0760-2

[42] B. Delley (2000) From molecules to solids with the $DMol^3$ approach, J. Chem. Phys. 113:7756-7764. https://doi.org/10.1063/1.1316015

[43] H. Luo, H. Li, Q. Fu (2017) First-principles study of l-cysteine adsorption on vacancy graphene and Ag-doped graphene, Comp. Mater. Sci. 127:222-229. https://doi.org/10.1016/j.commatsci.2016.11.004

[44] S. Grimme (2006) Semiempirical GGA-type density functional constructed with a long-range dispersion correction, J. Comput. Chem. 27:1787-1799. https://doi.org/10.1002/jcc.20495

[45] D. Ma, W. Ju, T. Li, G. Yang, C. He, B. Ma, Y. Tang, Z. Lu, Z. Yang (2016) Formaldehyde molecule adsorption on the doped monolayer MoS_2: A first-principles study, Appl. Surf. Sci. 371:180-188. https://doi.org/10.1016/j.apsusc.2016.02.230

[46] J.L. Fajin, J.R. Gomes, M.N. Cordeiro (2013) DFT Study of the Adsorption of $_{D\text{-}(L\text{-})}$Cysteine on Flat and Chiral Stepped Gold Surfaces, Langmuir 29:8856-8864. https://doi.org/10.1021/la401057f

[47] B. Höffling, F. Ortmann, K. Hannewald, F. Bechstedt (2010) Single cysteine adsorption on Au(110): A first-principles study, Phys. Rev. B 81:045407. https://doi.org/10.1007/978-3-642-23869-7_9

[48] L.H. Yao, M.S. Cao, H.J. Liu, X.Y. Fang, J. Yuan (2014) Adsorption of Na on intrinsic, B-doped, N-doped and vacancy graphenes: A first-principles study, Comp. Mater. Sci. 85:179-185. https://doi.org/10.1016/j.commatsci.2013.12.052

[49] B. Cordero, V. Gomez, A.E. Platero-Prats, M. Reves, J. Echeverria, E. Cremades, F. Barragan, S. Alvarez (2008) Covalent radii revisited†‡, Dalton Trans. 37:2832-2838. https://doi.org/10.1039/B801115J

[50] C. Kittel, Introduction to Solid State Physics, 7th edition, Wiley, New York, 1996, 57.

[51] K. Iyakutti1, E.M. Kumar, R. Thapa, R. Rajeswarapalanichamy, V.J. Surya, Y. Kawazoe (2016) Effect of multiple defects and substituted impurities on the band structure of graphene: a DFT study. J. Mater. Sci. Mater. El. 27: 12669-12679. https://doi.org/10.1007/s10854-016-5401-9

[52] H. Wang, Q. Wang, Y. Cheng, K. Li, Y. Yao, Q. Zhang, C. Dong, P. Wang, U. Schwingenschlogl, W. Yang, X.X. Zhang (2012) Doping Monolayer Graphene with Single Atom Substitutions. Nano Lett. 12:141-144. https://doi.org/10.1021/nl2031629

[53]https://en.wikipedia.org/wiki/Ionization_energy.